Strain-Induced Slater Transition in Polar Metal LiOsO₃

Yu Zhang, Ji-Jun Gong, Chuan-Fu Li, Lin Lin, Zhi-Bo Yan, Shuai Dong,*
and Jun-Ming Liu

LiOsO₃ is the first experimentally confirmed polar metal. Previous works suggested that the ground state of LiOsO₃ is just close to the critical point of metal–insulator transition. Herein, the electronic state of LiOsO₃ is tuned by epitaxial biaxial strain, which undergoes the Slater-type metal–insulator transition under tensile strain, i.e., the G-type antiferromagnetism emerges. The underlying mechanism of bandwidth tuning can be extended to its sister compound NaOsO₃, which shows an opposite transition from an antiferromagnetic insulator to a nonmagnetic metal under hydrostatic pressure. A feasible route is suggested for the manipulation of magnetism and conductivity of polar metal LiOsO₃.

It is well known that metals cannot exhibit ferroelectric distortions because of the screening effects of the conduction electrons. However, in 1965, Anderson and Blount suggested that the loss of inversion symmetry could occur in metallic materials through a continuous structural transition so that polar metals could exist.[1] The first success in the experimental findings of polar metals is LiOsO₃, which was reported to undergo a second-order structural phase transition from the centrosymmetric structure (space group $R\bar{3}c$) to the noncentrosymmetric structure (space group $R3c$) at temperature $T = 140$ K with metallic behavior unchanged.[2]

The novel properties of polar metals have attracted much attention since the first experimental report about LiOsO₃ in 2013. The major concerns of LiOsO₃ are not only the potential applications but also, more importantly, possible couplings between the ferroelectricity and metallicity which are usually mutually exclusive. Many efforts have been devoted into understanding the origin of the ferroelectric-like distortion in the metallic state of LiOsO₃, and the microscopic mechanism has

Y. Zhang, Dr. J.-J. Gong, C.-F. Li, Dr. L. Lin, Dr. Z.-B. Yan, Prof. J.-M. Liu
Laboratory of Solid State Microstructures
Nanjing University
Nanjing 210093, China

Prof. S. Dong
School of Physics
Southeast University
Nanjing 211189, China
E-mail: sdong@seu.edu.cn

Prof. J.-M. Liu
Institute for Advanced Materials
Hubei Normal University
Huangshi 435002, China

The ORCID identification number(s) for the author(s) of this article can be found under https://doi.org/10.1002/pssr.201900436.

been investigated.[3–6] Although several previous experimental and theoretical studies have demonstrated the primary issues of polar metals, the physics of LiOsO₃ is still puzzling and controversial.[2,7–9]

Previous works based on both local density approximation (LDA) $+ U$ and LDA + dynamic meaning field theory (DMFT) suggested that the ground state of LiOsO₃ is just located near the critical point of metal–insulator transition.[10] If the Coulomb repulsion of Os⁵⁺ is weak enough, the strong hybridization between Os's 5d and O's 2p orbitals and spin–orbit coupling (SOC) will suppress the local magnetic moment in LiOsO₃ completely and then the ground state should be metallic. But if the Coulomb repulsion is significant, a G-type antiferromagnetic (G-AFM) structure would be established with every nearest-neighboring spins oppositely aligned, and meanwhile LiOsO₃ will become an insulator. For the half-filling t_{2g} orbital of Os⁵⁺, the Hubbard U will ideally split the t_{2g} orbitals into full-filled lower Hubbard bands and empty upper Hubbard bands, with the opposite signs of periodic potential on each nearest neighbor, i.e., the Slater-type metal–insulator transition (see Figure S1, Supporting Information).[11]

Up to now, all experimental evidences showed that LiOsO₃ should be a nonmagnetic (NM) weak-correlated metal, which is different from other 5d³ osmium oxides such as NaOsO₃, Cd₂OsO₇, etc.[12–14] As clarified in a previous study,[10] the main factor that makes LiOsO₃ different from NaOsO₃ is the difference between their lattice structures. The Os–O–Os network is more compact in LiOsO₃ than that in NaOsO₃, so the 5d–2p hybridization is stronger and the effective hopping between the nearest-neighbor Os's 5d orbitals is larger in LiOsO₃ than that in NaOsO₃. Hence, the bandwidths of 5d orbitals in LiOsO₃ are relatively wider than those in NaOsO₃. Then the narrower 5d bands of NaOsO₃ favor a stable G-AFM structure.

Then it is natural to expect that the suppressed magnetic ordering of LiOsO₃ could be revived by reducing the kinetic energy of 5d electrons which enhances the electron localization. Puggioni et al. proposed a strategy of electronic structure control in LiOsO₃ by enhancing the electronic correlations in the LiOsO₃ layers of an ultrashort period LiOsO₃/LiNbO₃ superlattice, and their calculation showed that the insulating and magnetic state of LiOsO₃ could be driven by the reduction in bandwidth of t_{2g} orbitals in the superlattice geometry.[15]

In this article, we will consider a simpler route, i.e., to apply biaxial strains, to tune the distances between ions in the Os–O–Os network of LiOsO₃. Then under the tensile case, the itinerant electrons should be more localized and the

ADVANCED
SCIENCE NEWS
www.advancedsciencenews.com

pss rrl
physica status solidi
www.pss-rapid.com

magnetic order is expectable. Although the strain effects were addressed before, the magnetism was neglected.[16,17] Using the first-principles density functional theory (DFT), our calculation reveals that $LiOsO_3$ will turn into G-AFM insulator with the unchanged crystal symmetry under tensile biaxial strain. Our results suggest an alternative route for the manipulation of the physical properties and functionality of $LiOsO_3$.

The DFT calculations are performed using the pseudopotential plane-wave method as implemented in Vienna Ab initio Simulation Package (VASP).[18–20] The electron interactions are described using the Perdew–Burke–Ernzerhof (PBE) of the generalized gradient approximation (GGA).[21] The projected augmented wave (PAW)[22] pseudopotentials with a 500 eV plane-wave cutoff are used, including three valence electrons for Li $(1s^2 2s^1)$, nine for Na $(2s^2 2p^6 3s^1)$, fourteen for Os $(5p^6 6s^2 5d^6)$, and six for O $(2s^2 2p^4)$. Starting from the experimental structures, the lattice constants and all atomic coordinates are fully relaxed within the initial space group, until the Hellman–Feynman forces on every atom are converged to less than 1.0 meV $Å^{-1}$. A $13 \times 13 \times 7$ mesh for the cell of $LiOsO_3$ in $R3c$ hexagonal phase (containing 30 atoms) and a $13 \times 13 \times 13$ mesh for the unit cell of $NaOsO_3$ are used for the Brillouin-zone sampling.

The Coulomb repulsion in correlated electron systems is usually characterized by the on-site Hubbard U. As the Coulomb repulsion should be insignificant in 5d systems because of the spatially extended 5d orbitals, we have carefully investigated the ground state of $LiOsO_3$ by performing two different types of DFT + U methods[10]: the LDA + U method introduced by Liechtenstein et al. in which the exchange splitting J and the Hubbard U are considered separately and the simplified local spin density approximate (LSDA) + U method introduced by Dudarev et al. which only needs a parameter $U_{eff} = U - J$.[23,24] In the LDA + U case, the suitable value of Hubbard U in $LiOsO_3$ should be in the range of 1.0–2.0 eV, but in LSDA + U case, the value of U_{eff} should be small enough (≈ 0 eV), i.e., a bare LSDA calculation is a proper choice.

In our calculations, the space groups are kept unchanged upon the external strain or pressure, i.e., structural transition is not considered although it may occur in some cases.[25,26] To guarantee this assumption, the dynamic stability of the lattice will be checked using its phonon spectrum as well as the elastic coefficients[27] (Figure S2, Supporting Information). The ferroelectric polarization for the insulating state is calculated using the Berry phase method.[28,29] The total spontaneous polarization P for a given crystalline symmetry can be calculated as the sum of ionic and electronic contributions.

We take the hexagonal cell of $LiOsO_3$ in the noncentrosymmetric phase of $R3c$ as the reference structure, as shown in **Figure 1**a. First, previous works have proved that the magnetic phase of $LiOsO_3$ could only be NM or G-AFM whatever the condition is.[3,9,10,15] So in the following, we only consider the competition between the NM phase and G-AFM phase. The total and partial density of states (DOS) are shown in Figure 1b,c. As expected, $LiOsO_3$ is insulating in the G-AFM state, whereas the NM state is metallic. For both cases, Os's 5d orbitals and O's 2p orbitals are overlapped around the Fermi level, suggesting the strong hybridization between them. Due to the crystalline electric field, the Os's 5d orbitals are split into the t_{2g} triplet manifold and e_g doublet manifold. Thus the magnetic configuration will be formed by the total moment of the half-filled t_{2g} orbitals of Os^{5+}.

To reduce the t_{2g} bandwidth of Os^{5+} via making the Os–O–Os network looser, we consider applying biaxial strain which can be achieved in experiments by epitaxial growth techniques. In crystals with $R3c$ space group, the lattice parameter a equals the lattice parameter b. The a/b plane biaxial strain is defined as $\varepsilon = (a - a_0)/a_0$, where a_0 is the optimized lattice parameter for the fully relaxed $LiOsO_3$. We study the ground state of $LiOsO_3$ under an appreciable range of strains, from -5% to 5%, whereas the negative numbers represent compressive strain and the positive numbers represent tensile strain. With constrained a/b, the out-of-plane lattice parameter c and internal atomic coordinates are fully relaxed, and the crystal symmetry of the $LiOsO_3$ cell is kept unchanged at the $R3c$ space group during the optimized process (whose stability is further verified, see Figure S2, Supporting Information).

To accurately confirm the magnetic order of $LiOsO_3$ under biaxial strains, first we perform the LSDA + SOC calculation
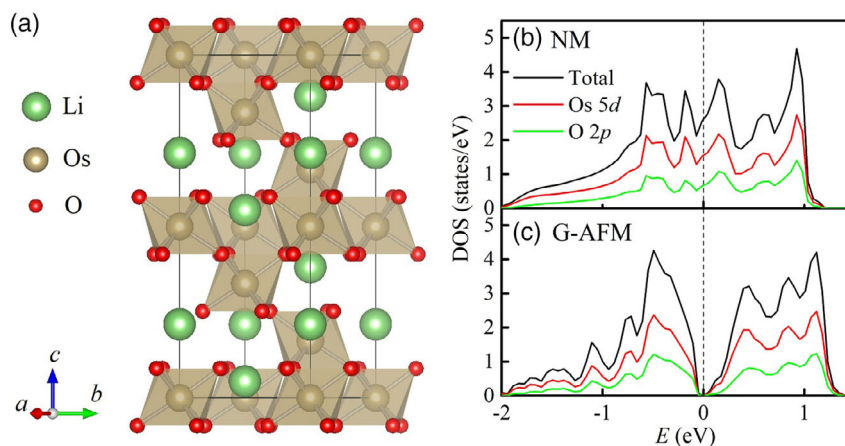
Figure 1. a) The hexagonal crystal structure of $LiOsO_3$ in noncentrosymmetric phase. The total and partial density of states (DOS) of $LiOsO_3$ (per f.u.) in b) NM state and c) G-AFM state, calculated by LSDA.

ADVANCED SCIENCE NEWS
www.advancedsciencenews.com

pss rrl
physica status solidi
www.pss-rapid.com

on LiOsO$_3$; here, the SOC is considered because several works have found that SOC may play a significant role in the magnetic properties of 5d osmium oxides.[14,30–32] We compare the total energy of LiOsO$_3$ cell in the NM state and G-AFM state. The results are shown in **Figure 2**a–c. We can see that the energy difference between the total energy of LiOsO$_3$ cell in the NM state and G-AFM state varies with the magnitude of strain. As shown in Figure 2a, the total energy of LiOsO$_3$ in the NM state would gradually go beyond that in the G-AFM state as the magnitude of strain increases, which means the ground state of LiOsO$_3$ turns from the NM phase to G-AFM phase. Within a certain range of tensile strain ($\approx$>2%), the G-AFM state would be the most stable for LiOsO$_3$. In other cases, the ground state of LiOsO$_3$ would remain in the NM state. In practice, the possible substrate candidates may be LiTaO$_3$ ($\approx$2.15% larger) or the (111) surface of LaAlO$_3$ or YAlO$_3$ (6.1% or 3.8% larger). The magnetic moment and band gap also grow with the tensile strain, as shown in Figure 2b,c, indicating that the G-AFM phase becomes more and more stable as the magnitude of tensile strain increases.

To reveal the underlying physical mechanism, the calculated structural parameters of LiOsO$_3$ as a function of strain are shown in Figure S3, Supporting Information. Under the tensile condition, the nearest-neighbor Os–Os distance (as well as Os–O–Os bond angle) becomes larger due to the expanded in-plane lattice constant although the out-of-plane lattice constant is shrunk. The compressive strain leads to the opposite tendency. Obviously, the longer Os–O bond and the larger distance

between the nearest-neighbor Os–Os pair reduce the orbital hybridization and thus the bandwidth.

To verify the mechanism of tensile strains, the partial DOS of 5d orbitals of each Os in the G-AFM state is shown in **Figure 3**a. Here, two cases are compared: unstrained and +3% tensile strained. As expected, the bandwidth of t_{2g} orbitals in the latter case is narrower that in the former case. So when the magnitude of tensile strain goes beyond the critical point, the 5d electrons of Os^{5+} tend to be localized and prefer to establish the G-AFM structure, which agrees with our expectation.

The linear optical properties of LiOsO$_3$ in the G-AFM state under tensile strains are also studied as a fingerprint of electronic structure. The calculated linear optical absorption coefficients before phase transition (undistorted) and after phase transition (+3% tensile strain) are shown in Figure S4, Supporting Information. Two main absorption peaks exist: one is located between 1.0 and 1.3 eV, the other is located between 3.5 and 4.5 eV. The first absorption peak is probably caused by electron transition from O's 2p orbital below Fermi level to Os's t_{2g} orbital, and the second absorption peak may be caused by electron transition from O's 2p orbital to Os's e_g orbital. The valleys located between 2.2 and 2.5 eV should be attributed to the gap between e_g orbital and t_{2g} orbital. It is obvious that the location of absorption peak is red shifting under tensile strain, indicating that the energy level of Os's 5d orbital is decreasing. This feature confirms that tensile strain could make the bandwidth of 5d orbitals narrower as we expected.

In addition to aforementioned LSDA calculations, we also perform LDA + U calculation on strained LiOsO$_3$ (the magnitude of strain is set to +3%) to confirm that our results are not dependent on particular computing methods. We set $J/U = 0.25$ and
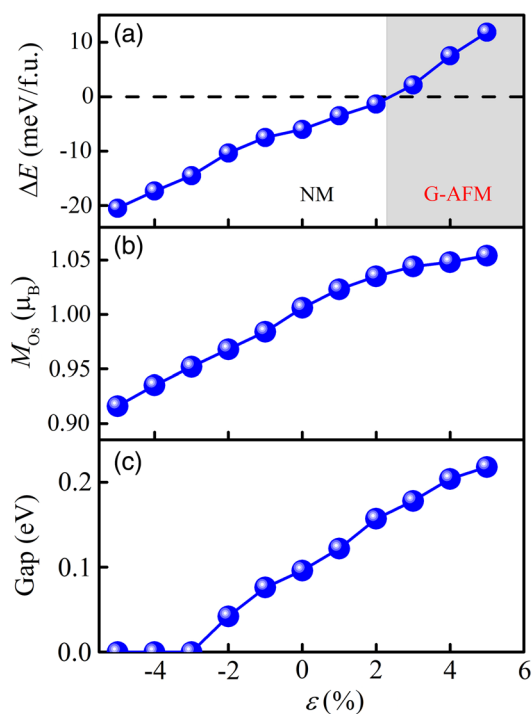
Figure 2. Results of LSDA+SOC calculations for LiOsO$_3$ as a function of biaxial strain ε. Negative values represent compressive strains, and positive values represent tensile strains. a) The energy difference between the G-AFM state and NM state ($\Delta E = E_{NM} - E_{G\text{-}AFM}$). b) The magnetic moment of Os ion in the G-AFM state. c) The band gap of LiOsO$_3$ in the G-AFM state.
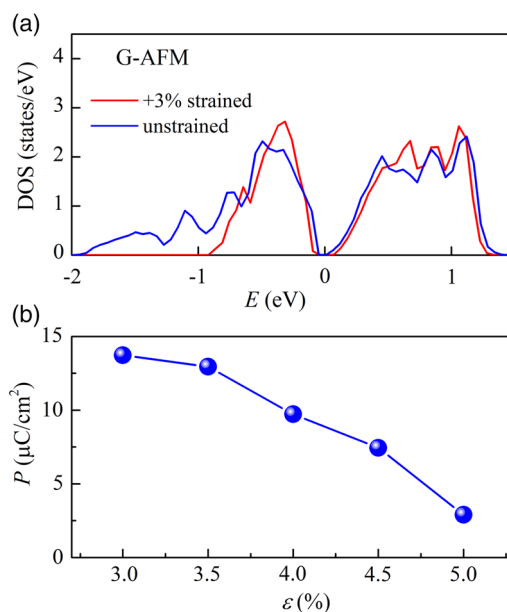
Figure 3. a) The partial DOS of each Os in the G-AFM state of LiOsO$_3$ (per f.u.): unstrained and +3% tensile strained, calculated by LSDA. b) The calculated ferroelectric polarization (P) along the c axis as a function of biaxial strain ε.

restrict the range of U in 1.0–2.0 eV. The energy difference between the G-AFM phase and NM phase and the magnetic moment of Os^{5+} are shown in Figure S5, Supporting Information, as a function of U. In the LDA + U calculation, the tensile strain can enlarge the energy difference between G-AFM phase and NM phase and increase the local magnetic moment. Hence, both the LSDA calculation and LDA + U calculation reach the same conclusion.

As the G-AFM structure could open a gap in the Fermi level of $LiOsO_3$, we can calculate the spontaneous ferroelectric polarization in the noncentrosymmetric $LiOsO_3$ cell. The ferroelectric polarization is calculated using the Berry phase approach. The polarization is shown in Figure 3c as a function of strain, which decreases with the increasing magnitude of strain. Clearly, the polar displacements in $LiOsO_3$ will be reduced by tensile biaxial strains. This result is easy to be understood as the polar displacements in $LiOsO_3$ are predominantly along the c axis,[2] and thus the reduced lattice constant along the c axis suppresses the polarization.

Consequently, as we can manipulate the ground state of $LiOsO_3$ by applying tensile strain, then, could we change the G-AFM insulating phase in $NaOsO_3$ into NM metallic phase via compressive strain considering the similarities of their structures? Our calculation indeed predicts that such magnetic transition can occur when the biaxial compression is beyond -8% (Figure S6, Supporting Information), which may be too large in practice.

Considering the feasibility for experiment, we consider the hydrostatic pressure on $NaOsO_3$ crystal instead, which can reach a similar effect. We optimize the structure of $NaOsO_3$ under pressures and then study the magnetic and electronic properties at the ground state. As shown in **Figure 4**a, the ground state of $NaOsO_3$ would turn into NM metallic phase under a relatively large pressure (>35 GPa), whereas the crystal symmetry is kept unchanged (whose dynamic stability is further verified according to the elastic coefficients. See SM for more details). Even for the G-AFM state, the pressure can suppress the local magnetic moment, as shown in Figure 4b. We compare the partial DOS of the undistorted cell with the one under 50 GPa, as shown in Figure 4c, which indicates that the bandwidths of 5d orbitals are clearly wider under pressure. That means the applied hydrostatic pressure makes the Os–O–Os network more compact so that the 5d electrons will be more delocalized and the effective hopping between the nearest-neighbor Os–Os pair's 5d orbitals is larger, eventually leading to the quenching of the local moment of Os^{5+} ($5d^3$) in $NaOsO_3$.

In summary, we have performed first-principles calculations to study the effects of biaxial strains on $LiOsO_3$. It is revealed that the ground state of $LiOsO_3$ would change from NM metal into G-AFM insulator under tensile biaxial strain. This magnetic phase transition would cause a Slater-type metal–insulator transition. The physical mechanism for the strain-induced phase transition in $LiOsO_3$ can also be applied to $NaOsO_3$. In contrast, the ground state of $NaOsO_3$ would turn from G-AFM insulator into NM metal under sufficiently large hydrostatic pressure. Our results suggest a feasible way to manipulate the electronic and magnetic properties of polar metal $LiOsO_3$. Our work would motivate new applications of polar metal materials.
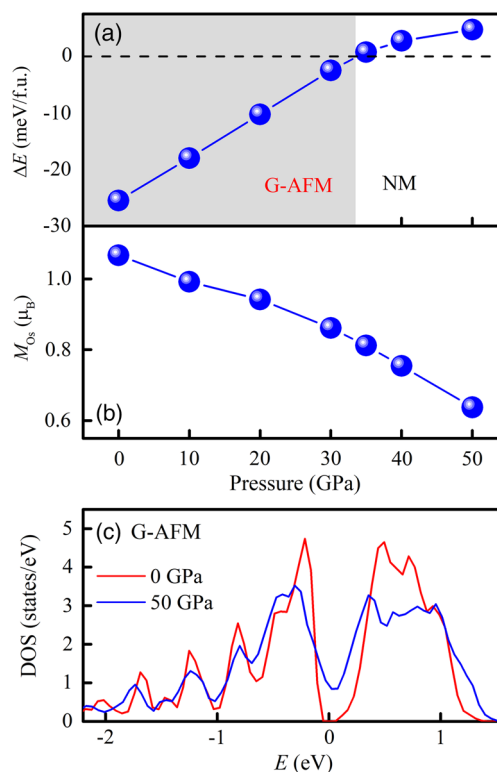
Figure 4. Results of LSDA + SOC calculations for $NaOsO_3$ as a function of applied hydrostatic pressure and partial DOS patterns in two cases. a) The energy difference between NM state and G-AFM state ($\Delta E = E_{G\text{-AFM}} - E_{NM}$). b) The magnetic moment of Os ion in the G-AFM state. c) Partial DOS (per f.u.) of Os's 5d orbitals for the original one and the compressed one with 50 GPa hydrostatic pressure.

Supporting Information

Supporting Information is available from the Wiley Online Library or from the author.

Conflict of Interest

The authors declare no conflict of interest.

[1] P. W. Anderson, E. I. Blount, *Phys. Rev. Lett.* **1965**, *14*, 217.

[2] Y. Shi, Y. Guo, X. Wang, A. J. Princep, D. Khalyavin, P. Manuel, Y. Michiue, A. Sato, K. Tsuda, S. Yu, M. A. Arai, *Nat. Mater.* **2013**, *12*, 1024.

[3] G. Giovannetti, M. Capone, *Phys. Rev. B* **2014**, *90*, 195113.

[4] H. Sim, B. G. Kim, *Phys. Rev. B* **2014**, *89*, 201107.

[5] H. J. Xiang, *Phys. Rev. B* **2014**, *90*, 094108.

[6] H. M. Liu, Y. P. Du, Y. L. Xie, J. M. Liu, C.-G. Duan, X. Wan, *Phys. Rev. B* **2015**, *91*, 064104.

[7] I. Lo Vecchio, G. Giovannetti, M. Autore, P. Di Pietro, A. Perucchi, J. He, K. Yamaura, M. Capone, S. Lupi, *Phys. Rev. B* **2016**, *93*, 161113.

[8] F. K. K. Kirschner, F. Lang, F. L. Pratt, T. Lancaster, Y. Shi, Y. Guo, A. T. Boothroyd, S. J. Blundell, *JPS Conf. Proc.* **2018**, *21*, 011013.

[9] C. He, Z. Ma, B.-Z. Sun, Q. Li, K. Wu, *Comput. Mater. Sci* **2015**, *105*, 11.

[10] Y. Zhang, J. Gong, C. Li, L. Lin, Z. Yan, S. Dong, J.-M. Liu, *Phys. Status Solidi RRL* **2018**, *12*, 1800396.

[11] J. C. Slater, *Phys. Rev.* **1951**, *82*, 538.

[12] S. Calder, V. O. Garlea, D. F. McMorrow, M. D. Lumsden, M. B. Stone, J. C. Lang, J. W. Kim, J. A. Schlueter, Y. G. Shi, K. Yamaura, Y. S. Sun, *Phys. Rev. Lett.* **2012**, *108*, 257209.

[13] Y. G. Shi, Y. F. Guo, S. Yu, M. Arai, A. A. Belik, A. Sato, K. Yamaura, E. Takayama-Muromachi, H. F. Tian, H. X. Yang, J. Q. Li, *Phys. Rev. B* **2009**, *80*, 161104.

[14] S. Calder, J. G. Vale, N. A. Bogdanov, X. Liu, C. Donnerer, M. H. Upton, D. Casa, A. H. Said, M. D. Lumsden, Z. Zhao, J. Q. Yan, *Nat. Commun.* **2016**, *7*, 11651.

[15] D. Puggioni, G. Giovannetti, M. Capone, J. M. Rondinelli, *Phys. Rev. Lett.* **2015**, *115*, 087202.

[16] Q. Yao, H. Wu, K. Deng, E. Kan, *RSC Adv.* **2014**, *4*, 26843.

[17] E. I. P. Aulestia, Y. W. Cheung, Y.-W. Fang, J. He, K. Yamaura, K. T. Lai, S. K. Goh, H. Chen, *Appl. Phys. Lett.* **2018**, *113*, 012902.

[18] G. Kresse, J. Hafner, *Phys. Rev. B* **1993**, *47*, 558.

[19] G. Kresse, J. Furthmüller, *Phys. Rev. B* **1996**, *54*, 11169.

[20] G. Kresse, J. Furthmüller, *Comput. Mater. Sci.* **1996**, *6*, 15.

[21] J. P. Perdew, K. Burke, M. Ernzerhof, *Phys. Rev. Lett.* **1996**, *77*, 3865.

[22] P. E. Blöchl, *Phys. Rev. B* **1994**, *50*, 17953.

[23] A. I. Liechtenstein, V. I. Anisimov, J. Zaanen, *Phys. Rev. B* **1995**, *52*, R5467.

[24] S. L. Dudarev, G. A. Botton, S. Y. Savrasov, C. J. Humphreys, A. P. Sutton, *Phys. Rev. B* **1998**, *57*, 1505.

[25] A. J. Hatt, N. A. Spaldin, C. Ederer, *Phys. Rev. B* **2010**, *81*, 054109.

[26] Z.-J. Wu, E.-J. Zhao, H.-P. Xiang, X.-F. Hao, X.-J. Liu, J. Meng, *Phys. Rev. B* **2007**, *76*, 054115.

[27] J.-G. Cheng, K. E. Kweon, J. S. Zhou, J. A. Alonso, P. P. Kong, Y. Liu, C. Jin, J. Wu, J. F. Lin, S. A. Larregola, W. Yang, *Proc. Natl. Acad. Sci. USA* **2013**, *110*, 20003.

[28] R. D. King-Smith, D. Vanderbilt, *Phys. Rev. B* **1993**, *47*, 1651.

[29] D. Vanderbilt, R. D. King-Smith, *Phys. Rev. B* **1993**, *48*, 4442.

[30] H. Shinaoka, T. Miyake, S. Ishibashi, *Phys. Rev. Lett.* **2012**, *108*, 247204.

[31] H. Matsuura, K. Miyake, *J. Phys. Soc. Jpn.* **2013**, *82*, 073703.

[32] A. E. Taylor, R. Morrow, R. S. Fishman, S. Calder, A. I. Kolesnikov, M. D. Lumsden, P. M. Woodward, A. D. Christianson, *Phys. Rev. B* **2016**, *93*, 220408.